Microchimica Acta (2025) 192:867
https://doi.org/10.1007/s00604-025-07745-2

RESEARCH

Molecularly imprinted electrochemical determination of cymoxanil fungicide by using bismuth incorporated bismuth vanadate nanocomposite

Şule Yıldırım Akıcı[1] · Sena Bekerecioğlu[1] · İlknur Polat[1] · Müge Mavioğlu Kaya[2] · Necip Atar[3] · Mehmet Lütfi Yola[4]

Received: 24 October 2025 / Accepted: 25 November 2025 / Published online: 29 November 2025

Abstract
Cymoxanil (CYM), an aliphatic nitrogen fungicide, is widely used in vegetables/fruits and it is effective against a diverse group of fungal pathogens. However, its long-term consumption can result in an important damage to human and environment such as acute poisoning. In present study, a molecularly imprinting electrochemical sensor based on bismuth incorporated bismuth vanadate (Bi-$BiVO_4$) nanocomposite was prepared and applied to CYM detection in orange and apple juice samples. After the preparation of the Bi-$BiVO_4$ nanocomposite by using environmentally friendly hydrothermal technique with minimal waste, the Bi-$BiVO_4$ nanocomposite modified electrode surface was developed by using IR lamp. CYM imprinted electrode based on Bi-$BiVO_4$ nanocomposite was prepared in the presence of CYM as analyte and pyrrole as monomer using cyclic voltammetry (CV). This sensor showed linear response of 1.0×10^{-9} – 1.0×10^{-8} mol L^{-1}, limit of quantification (LOQ) of 1.0×10^{-9} mol L^{-1}, and limit of detection (LOD) of 3.3×10^{-10} mol L^{-1}. The sensor system is environmentally friendly, fast-responding, and provides high accuracy and sensitivity compared to other conventional analytical methods. Finally, selectivity, stability and reproducibility of the sensor was highlighted and the sensor was applied to CYM detection in orange and apple juice samples with high recovery. In summary, thanks to the Bi-$BiVO_4$ nanocomposite presented for the first time in the literature for CYM fungicide determination, the successful implementation of the electrochemical sensor system has been demonstrated.

Keywords Cymoxanil · Nanocomposite · Molecularly imprinting polymer · Modified glassy carbon electrode · Voltammetry

Introduction

Fungicides are chemical or biological compounds used to prevent or destroy the growth of fungi and fungus-like organisms that cause disease in plants. These compounds can exert various effects by inhibiting spore germination and mycelial development or disrupting the integrity of the fungal cell membrane. Thus, they play an important role in maintaining plant health and ensuring sustainable product quality [1]. CYM, an agricultural fungicide, is used in the treatment of diseases caused by fungi of the order Peronosporales (especially Phytophthora infestans) in plants and belongs to the chemical class of cyanoacetamide-oxime derivatives and shows local, systemic and contact activities. It is particularly effective in inhibiting RNA and protein synthesis in fungal cells during the early stages of infection, thus stopping fungal growth and used against potato and tomato blight and in the treatment of mildew on tomatoes and grapes [2]. It is also preferred to control mildew, frost and late blight in legumes and many vegetable and fruit crops [3, 4]. A study has indicated that CYM residues were found in surface and groundwater in some regions in Spain [5]. According to the European Food Safety Authority

✉ Mehmet Lütfi Yola
mehmetlutfiyola@ankara.edu.tr

1 Department of Nutrition and Dietetics, Faculty of Health Sciences, Hasan Kalyoncu University, Gaziantep 27010, Türkiye, Turkey

2 Department of Molecular Biology and Genetic, Faculty of Art and Science, Kafkas University, 36000 Kars, Türkiye

3 Department of Chemical Engineering, Faculty of Engineering, Pamukkale University, Denizli 20160, Türkiye, Turkey

4 Department of Biology, Faculty of Science, Ankara University, Ankara 06100, Türkiye, Turkey

(EFSA), the ADI (Acceptable Daily Intake) value for CYM is stated as 0.013 mg/kg/day [6]. According to the USDA Pesticide Maximum Residue Limit (MRL) Database and the Foreign Agricultural Service, globally agreed tolerances for CYM residues range from 0.50 to 5.00 and 0.05 to 0.50 mg/kg, respectively. However, these values can vary for different crops in different countries [7].

As with all pesticides, CYM has been shown to exhibit toxic effects at certain levels and pose various risks to human health if exposed. The contact with eyes and skin can cause mild irritation, so the use of protective equipment is recommended. Systemic toxicity has been observed with high doses and long-term exposure to CYM. It has been reported to have mild degenerative effects, particularly on the kidneys and liver [8]. Additionally, some studies have shown that it can cause cardiotoxicity [9], reproductive problems, low birth weight, and energy deficiency [8].

Although CYM is a fungicide frequently used in agriculture, it leaves residue in plant tissues. In repeated and intensive applications of CYM, there is a risk of this fungicide being transferred into the food chain. The detection of CYM residues in produced foods is of great importance in ensuring food safety and protecting human health. In the literature, high-performance liquid chromatography tandem mass spectrometry (HPLC–MS/MS) [10], gas chromatography (GC-MS) [11] and high-performance liquid chromatography (HPLC) [12] are used for fungicide analysis. These analytical methods have been noted to have some drawbacks, such as lengthy sample preparation, high cost, and stability issues. Today, more sensitive, highly stable, economical, and time-saving methods are preferred over these analytical methods [13]. Electrochemical methods, which enable the analysis of a chemical type such as a pesticide, organic compound, metal ion, etc. by utilizing their electrical properties, have varieties such as voltammetry, amperometry and coulometry depending on the electrical quantity measured. The operating principle of all these methods is based on measuring the voltage/current changes that occur during redox reactions of a substance. Electrochemical methods offer the advantages of being fast, cost-effective, and highly selective and sensitive. With these features, electrochemical methods have been increasing in popularity in the last century, finding a wide range of applications, especially in areas such as food, environment and biotechnology [14, 15].

$BiVO_4$ belonging to high chemical stability has been investigated in some important applications such as electro-catalysis and pollutant determination [16]. In addition, $BiVO_4$ with a bandgap of 2.44 eV can increase the visible light efficiency and can be used in photoelectrochemical sensor detection [17]. Nonetheless, its efficiency is prevented via the limited carrier mobility and the fast carrier recombination and the low sensor signal responses is important problem to detect low amounts of analytes. To minimize this problem, several doping methods have been performed such as heterojunction formation, metal incorporation and co-catalyst preparation [18]. The doping of silver and gold nanoparticles resulting in surface plasmon resonance effect can carry out the improvement in light absorption and charge recombination. Nonetheless, due to the high cost of these silver and gold nanoparticles, some problems may occur in their intensive use. Especially, metallic bismuth shows the high catalytic activity resulting in the improved conductivity properties [19].

Molecular imprinting is a smart polymer synthesis process, which requires a template molecule, a functional monomer that interacts with the template molecule, and a solvent. The molecular imprinting process occurs in three steps. First, the template molecule and the functional monomer interact to form a complex, and then this complex structure is polymerized by the functional monomer. In the final step, the imprinted molecule is removed from the polymeric structure by washing, leaving a polymer with imprinted binding sites and high selectivity. Molecularly imprinted polymers (MIPs) containing specific binding sites are widely used in analysis, sensors, and various analytical applications due to their high specificity, economy, reusability, and durability [20, 21].

This study revealed a new perspective for fungicide-type pesticides by using Bi-$BiVO_4$ nanocomposite and molecularly imprinting polymer. The one-step hydrothermal technique with environmentally friendly property was used for the preparation of the nanocomposite. Hence, it was possible to say that the developed molecularly imprinting sensor had the features of a human and environment friendly sensor and applied to cymoxanil fungicide assay in orange and apple juice samples for the first time in the literature. Lastly, the early diagnosis of diseases resulting from fungicide exposure will be easier with this developed molecularly imprinting sensor.

Materials and methods

Materials

CYM, cyprodinil (CYP), mandipromamid (MAN), metalaxyl (MET), spiroxamine (SPI), pyrrole (Py) monomer, bismuth(III) nitrate ($Bi(NO_3)_3{\cdot}5H_2O$), ammonium metavanadate (NH_4VO_3), ethylene glycol ($C_2H_6O_2$) and phosphoric acid (H_3PO_4, ≥99.0%) as pH adjustment were purchased from Sigma-Aldrich Merck Group. Phosphate-buffered saline (pH 6.0, 0.1 mol L^{-1} PB) was selected as a supporting electrolyte.

Instrumentation

The apparatus for analytical and structural analyzes was presented in Supplementary Data.

Synthesis of $BiVO_4$ and Bi-$BiVO_4$ nanocomposite

The one-step hydrothermal technique was applied to the preparation of Bi-$BiVO_4$ nanocomposite. For this aim, the solution including $Bi(NO_3)_3 \cdot 5H_2O$ (2.0 mmol) and NH_4VO_3 (4.0 mmol) was prepared in pure-water (100.0 mL) including reducing agent $C_2H_6O_2$ (10.0 mL). After the reaction pH (about 4.5) was adjusted by slowly adding 0.1 mol L^{-1} H_3PO_4, the solution was put into Teflon autoclave. The heating treatment was applied to the solution at 200 °C for 5 h. After the cooling process, Bi-$BiVO_4$ nanocomposite was centrifuged and washed by pure-water. $BiVO_4$ was produced without incorporating $C_2H_6O_2$ as the base material and metallic bismuth was synthesized under the same conditions without $C_2H_6O_2$ as the substrate.

Preparation of Bi-$BiVO_4$ modified glassy carbon electrode (Bi-$BiVO_4$/GCE)

Our previous report was applied for the cleaning protocol of glassy carbon electrode (GCE) [22]. After the dropping treatment of Bi-$BiVO_4$ nanocomposite suspension (30.0 µL, 0.30 mg mL^{-1}) on the clean GCE surface, the GCE was dried by using IR lamp (Bi-$BiVO_4$/GCE). The development of $BiVO_4$/GCE for comparative experiments was performed by the same above procedure.

Development of CYM imprinted electrode and CYM removal

After the preparation of the electro-polymerization solution including 25.0 mmol L^{-1} CYM and 100.0 mmol L^{-1} Py, the nitrogen gas was passed through the electro-polymerization solution to remove the dissolved oxygen for 30 min. The high potential in range of 0.0/+1.0 V was applied to electrochemical cell including electro-polymerization solution by CV method and the electrochemical signals at about+0.70 V was monitored. During 25 scan cycles, CYM imprinted polymeric nanocavities were formed on Bi-$BiVO_4$/GCE and CYM imprinted Bi-$BiVO_4$/GCE was washed by pure-water and dried at 25 °C (MIP/Bi-$BiVO_4$/GCE). To demonstrate the high selectivity provided by molecular imprinting technology, NIP/Bi-$BiVO_4$/GCE was prepared by same above method without CYM molecule in existence of pH 6.0, 0.1 mol L^{-1} PB. Scheme 1 indicated the preparation stages of MIP/Bi-$BiVO_4$/GCE.

To maintain CYM removal from MIP/Bi-$BiVO_4$/GCE surface, 0.1 mol L^{-1} NaCl was used as the desorption (elution) solution. In non-covalent molecular imprinting processes, the removal of CYM molecule from the polymeric surface was not difficult because non-covalent interactions were weak, and the binding kinetics of the analyte molecule were faster. In this study, an ionic 0.1 mol L^{-1} NaCl solution was used as a desorption agent to eliminate the electrostatic and hydrogen bonding interactions between the polar groups of the Py monomer and CYM molecules. For this, MIP/Bi-$BiVO_4$/GCE was placed in a conical flask containing 0.1 mol L^{-1} NaCl and interacted for 20 min. Then, MIP/Bi-$BiVO_4$/GCE without CYM molecule was dried at 25 °C.

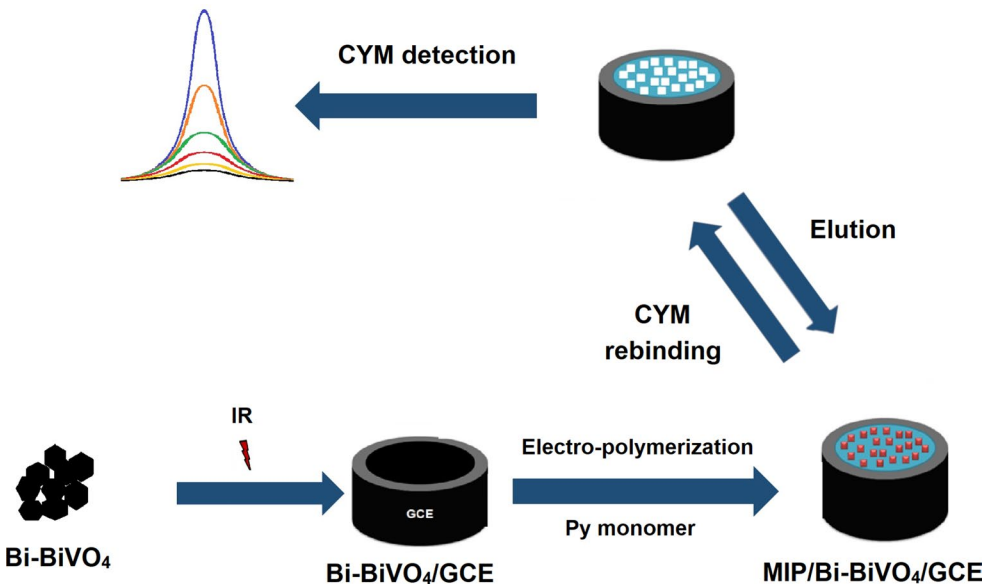

Scheme 1 Schematic display of MIP/Bi-$BiVO_4$/GCE preparation

Sample preparation

After the purchased orange and apple juice samples from the supermarket (10.0 mL) were separately transported into centrifuge tubes (50.0 mL), the centrifugation was carried out for 10 min to remove the residues in centrifuge tubes. Then, the solutions were diluted with pH 6.0, 0.1 mol L^{-1} PB to fall within the linearity range.

Results and discussion

Characterizations of Bi-$BiVO_4$ nanocomposite

The morphological investigations of $BiVO_4$ and Bi-$BiVO_4$ nanocomposite were firstly performed by SEM measurements (Fig. 1). According to Fig. 1A, the nanostructure like petal including two-dimensional confirmed the presence of $BiVO_4$ and the intercalation interactions between small bismuth and $BiVO_4$ were demonstrated on Fig. 1B, suggesting the uniform distribution of the aggregated bismuth on the surface of pristine $BiVO_4$ [17]. This situation revealed high surface-to-volume ratio belonging to Bi-$BiVO_4$ nanocomposite. Moreover, the presence of bismuth, oxygen, and vanadium verified the successful preparation of Bi-$BiVO_4$ nanocomposite (Fig. S1). In addition, the homogeneous dispersion profile belonging to bismuth incorporated bismuth vanadate nanocomposite was shown by EDX and SEM images [17].

The microstructure of Bi-$BiVO_4$ nanocomposite was confirmed by TEM image (Fig. 2). According to Fig. 2A, a sheet-like morphology with the curved structures and tiny bismuth particles including a diameter of about 4–8 nm was shown. Furthermore, Fig. 2B and C showed the enlarged TEM images belonging to metallic bismuth and bismuth incorporated bismuth vanadate nanocomposite, suggesting the obvious interaction between metallic bismuth and $BiVO_4$ [23]. In addition, the lattice spacing of 0.148 nm belonging to metallic bismuth in the nanocomposite (Fig. 2B) and the lattice spacing of 0.323 nm belonging to pristine $BiVO_4$ in the nanocomposite (Fig. 2C) were corresponded to (122) plane of metallic Bi and (121) plane of pristine $BiVO_4$, respectively.

XRD pattern of metallic Bi, pristine $BiVO_4$ and Bi-$BiVO_4$ nanocomposite was given on Fig. S2. XRD peaks at 22.57°, 26.94°, 38.03°, 40.11°, 49.17°, 55.43°, 61.93° and 64.53° were attributed to (003), (012), (104), (110), (202), (024), (116) and (122) planes of metallic Bi [24]. After the incorporation of metallic Bi into pristine $BiVO_4$, XRD peaks at 19.07°, 29.12°, 29.27°, 35.21°, 42.76°, 53.37° and 57.93° were corresponded to (011), (-121), (121), (002), (051), (-161) and (-321) planes of pristine $BiVO_4$, respectively [25], suggesting the successful incorporation of metallic Bi into pristine $BiVO_4$ with highly crystalline.

XPS experiments metallic Bi, pristine $BiVO_4$ and Bi-$BiVO_4$ nanocomposite for element chemical compositions were carried out (Fig. 3). According to the survey spectra (Fig. 3A), the presence of bismuth, oxygen, and vanadium confirmed the successful preparation of Bi-$BiVO_4$ nanocomposite. XPS peaks at 159.16 and 164.17 eV were attributed to Bi4f7/2 and Bi4f5/2, respectively, confirming the presence of Bi^{3+} and metallic Bi and suggesting the successful

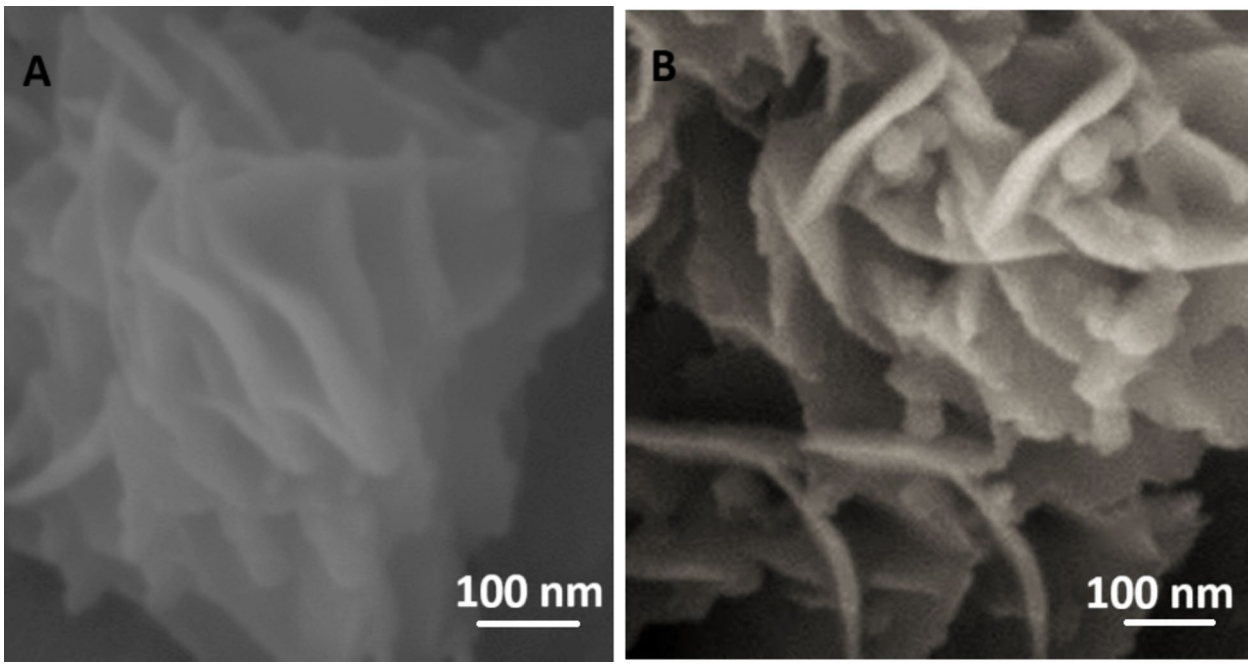

Fig. 1 SEM image of (**A**) $BiVO_4$ and (**B**) Bi-$BiVO_4$ nanocomposite

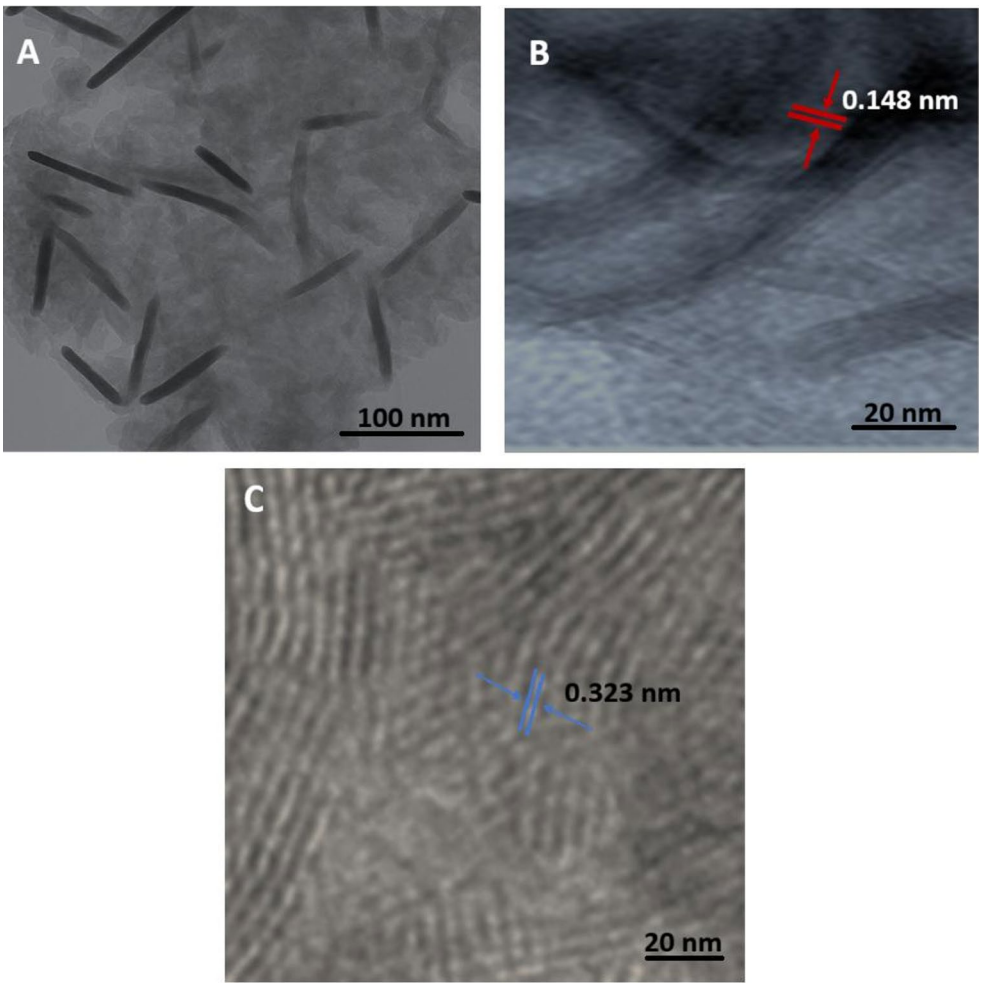

Fig. 2 (**A**) TEM image of Bi-$BiVO_4$ nanocomposite and the enlarged TEM images of (**B**) metallic Bi and (**C**) pristine $BiVO_4$

incorporation of metallic Bi into pristine $BiVO_4$ (Fig. 3B) [26]. In addition, the binding energy of Bi4f in pristine $BiVO_4$ was slightly shifted to the higher values compared with that of Bi-$BiVO_4$ nanocomposite. XPS spectrum of V2p (Fig. 3C) showed two chemical states attributing to V^{5+} (515.87 eV for V2p3/2 and 524.09 eV for V2p1/2) and V^{4+} (515.73 eV for V2p3/2 and 521.88 eV for V2p1/2), respectively and XPS peak intensity of V^{4+} was higher than that of V^{5+}, suggesting that more V^{4+} could be located in nanocomposite. In addition, the binding energy of V2p in pristine $BiVO_4$ shifted to the higher values compared with that of Bi-$BiVO_4$ nanocomposite in harmony with Bi4f. According to O1s XPS spectrum (Fig. 3D), the binding energy at 529.16 eV was attributed to $O_{lattice}$ in pristine $BiVO_4$ and XPS peaks at 530.61and 530.93 eV were corresponded to the hydroxyl and surface adsorbed water, respectively [17, 25].

Electrochemical studies of pristine $BiVO_4$ and Bi-$BiVO_4$ nanocomposite modified electrodes

The electrochemical activities of pristine $BiVO_4$ and Bi-$BiVO_4$ nanocomposite were examined by CV (Fig. 4A) and EIS (Fig. 4B) methods in existence of 1.0 mmol L^{-1} $[Fe(CN)_6]^{3-/4}$. Bare GCE with peak potential separation (ΔEp = 50 mV) demonstrated obvious anodic/cathodic peak. Then, an important catalytic enhancement with narrower potential separation (ΔEp = 40 mV) was obtained in anodic/cathodic peak signals on $BiVO_4$/GCE because of $BiVO_4$'s chemical stability [27]. The observed highest electrochemical signals and narrowest peak potential separation (ΔEp = 25 mV) via Bi-$BiVO_4$/GCE were due to easier charge recombination resulting from bismuth incorporation into the pristine $BiVO_4$ [28]. Hence, bismuth incorporation into the pristine $BiVO_4$ can provide greater adsorption of the analyte molecule on the electrode surface, showing the increased electrochemical activity. Secondly, EIS (Fig. 4B) was conducted to investigate the charge transport properties of Bi-$BiVO_4$/GCE and $BiVO_4$/GCE. Typically, a smaller semicircle radius signified the faster interfacial charge transfer. Hence, Bi-$BiVO_4$/GCE (curve c) demonstrated an importantly reduced semicircle radius in comparison with $BiVO_4$/GCE (curve b), indicating the superior interfacial charge transport. As expected, bare GCE (curve a) had the highest semicircle radius. Hence, while the charge transfer

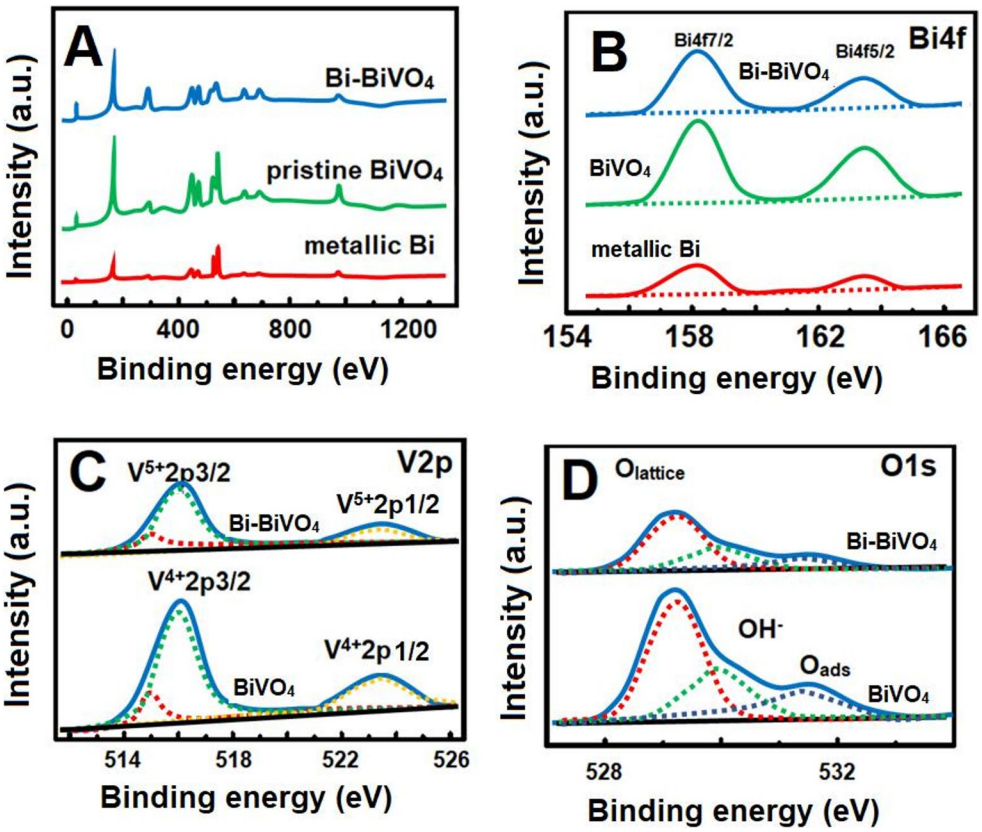

Fig. 3 XPS spectra of (**A**) survey, (**B**) Bi4f, (**C**) V2p and (**D**) O1s for metallic Bi, pristine $BiVO_4$ and Bi-$BiVO_4$ nanocomposite

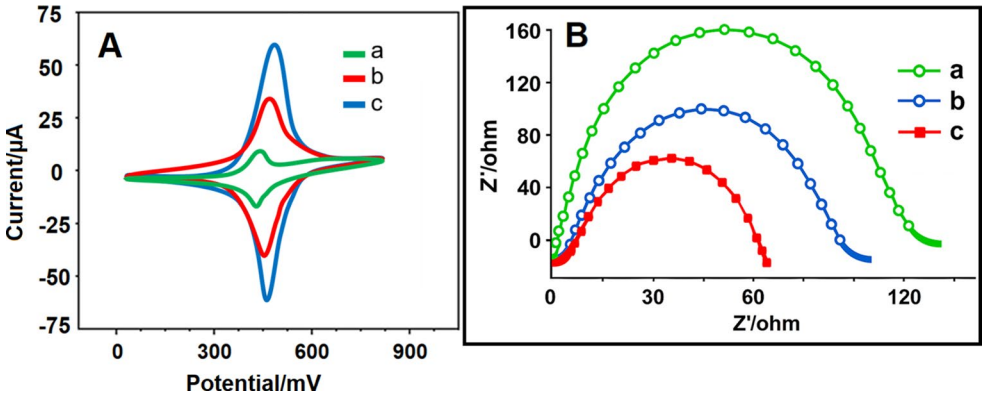

Fig. 4 (**A**) CV curves and (**B**) EIS responses at (a) bare GCE, (b) $BiVO_4$/GCE, (c) Bi-BiVO/GCE (Redox probe: 1.0 mmol L^{-1} $[Fe(CN)_6]^{3-/4-}$ containing 0.1 mol L^{-1} KCl, potential scan rate: 100 mV s^{-1})

resistance (Rct) was highest on the bare GCE electrode surface, the lowest Rct was on the Bi-$BiVO_4$/GCE electrode surface in harmony with CV results. The decrease in charge transfer resistance was also equivalent to the improvement of electroactive surface area and the electroactive surface areas of bare GCE, $BiVO_4$/GCE and Bi-$BiVO_4$/GCE were recorded as 0.070 ± 0.006, 0.467 ± 0.002 and 0.906 ± 0.005 cm^2 via $i_p = 2.69 \times 10^5$ A $n^{3/2}$ $D^{1/2}$ C $v^{1/2}$ equation in existence of 1.0 mmol L^{-1} $[Fe(CN)_6]^{3-}$, respectively. Hence, these results showed that the charge transfer resistance decreased with increasing electrode surface area.

To verify the diffusion controlled electrochemical mechanism, a linear dependency was obtained between the anodic and cathodic currents and the square root of the scan rate over the range of 10–500 mV s^{-1}, confirming that Bi-$BiVO_4$/GCE had diffusion controlled. The following linear regression equations were presented below:

$$\mathrm{Ipa} = 6.3179(\mathrm{v})^{1/2} + 5.0793\ (\mathrm{R}^2 = 0.9997)$$

$$\mathrm{Ipc} = -6.7917(\mathrm{v})^{1/2} - 4.2791\ (\mathrm{R}^2 = 0.9995)$$

Finally, the anodic and cathodic potentials shifted to positive and negative potentials, respectively, with increasing the scan rate, revealing typical quasi-reversible electron transfer on Bi-$BiVO_4$/GCE.

Development of CYM imprinted polymer on Bi-$BiVO_4$/GCE

The voltammograms relating to electro-polymerization in existence of 100.0 mmol L^{-1} Py monomer and 25.0 mmol L^{-1} CYM on Bi-$BiVO_4$/GCE were recorded on Fig. 5A in range of +0.0/+1.0 V. It was observed that the intensity of the distinct polymerization peak at approximately +0.70 V in the first scan decreased towards the end of the 25th scan. This showed that CYM imprinted polymeric nano-surface was formed on Bi-$BiVO_4$/GCE surface.

To demonstrate the high sensitivity advantage offered by molecular imprinting technology, as described in previous sections, the prepared MIP and NIP electrodes were separately treated with 10.0 nmol L^{-1} CYM in 0.1 mol L^{-1} PBS (pH 6.0). The electrochemical signals, invisible in the absence of CYM analyte, emerged at approximately 9.5 µA on MIP/Bi-$BiVO_4$/GCE and at approximately 1.0 µA on NIP/Bi-$BiVO_4$/GCE. The results showed that the MIP electrode recognized the CYM analyte with a sensitivity of approximately 9.5 times greater than the NIP electrode (Fig. 5B). Finally, the advantage of bismuth doping was demonstrated by interacting the prepared different MIP electrodes with 10.0 nmol L^{-1} CYM in 0.1 mol L^{-1} PBS (pH 6.0) (Fig. 5C). The electrochemical signals emerged at approximately 9.5 µA on MIP/Bi-$BiVO_4$/GCE and at approximately 5.0 µA on MIP/$BiVO_4$/GCE. In accordance with the CV and EIS results given in Sect. 3.2, it was observed that the highest electrochemical signals were obtained on MIP/Bi-$BiVO_4$/GCE electrode surface with bismuth doping.

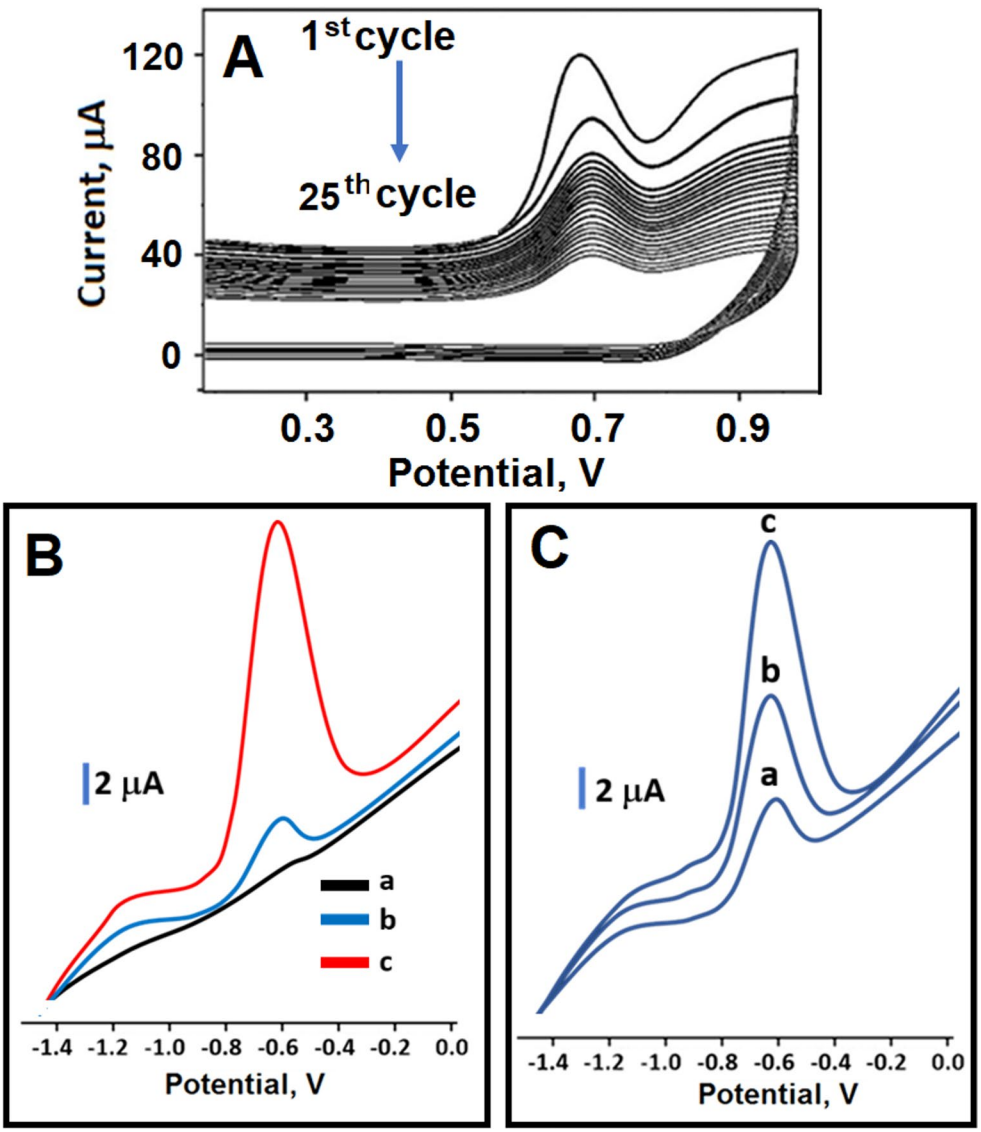

Fig. 5 (**A**) Electro-polymerization voltammograms in 100.0 mmol L^{-1} Py monomer and 25.0 mmol L^{-1} CYM on Bi-$BiVO_4$/GCE (Scan rate: 100 mV s^{-1}); (**B**) SWVs of the prepared electrodes in this study: (a) MIP/ Bi-$BiVO_4$/GCE in blank buffer solution (pH 6.0), (b) NIP/Bi-$BiVO_4$/GCE after rebinding of 10.0 nmol L^{-1} CYM in 0.1 mol L^{-1} PBS (pH 6.0), (c) MIP/Bi-$BiVO_4$/GCE after rebinding of 10.0 nmol L^{-1} CYM in 0.1 mol L^{-1} PBS (pH 6.0); (**C**) SWVs of different molecularly imprinting electrodes after rebinding of 10.0 nmol L^{-1} CYM in 0.1 mol L^{-1} PBS (a) MIP/bare GCE, (b) MIP/$BiVO_4$/GCE and (c) MIP/Bi-$BiVO_4$/GCE

Optimization

pH effect

According to Fig. S3A, the obvious decreases were observed in current signals in alkaline medium (pH 6.0–9.0). This situation indicated that the protonated CYM species were involved in electrochemical process. Moreover, the peak potential values shifted to more negative potentials in pH 4.0–6.0 range, confirming hydrogen ion participation in electrochemical process. For pH 4.0–6.0 range, the linear regression equation was obtained as Ep (V) = 0.445 + 0.059 pH. Above pH 7.0, a plateau was reached in harmony with pKa of CYM (pKa = 9.7) in terms of the peak potential values. Thus, the optimum pH value was selected as 6.0. In addition, hydrolysis of CYM molecules was limited at pH values close to neutral [13].

Mole ratio CYM to Py monomer effect

In molecularly imprinted electrochemical sensor applications, the thickness of the prepared electrode surface and the analyte and monomer concentrations affecting this thickness were significant. In particular, it was necessary to prepare a pre-complex that had maximum interaction on the electrode surface by optimizing the analyte: monomer ratio. If the monomer ratio was low enough, the stability of the prepared pre-complex could be low and it was difficult to imprint the analyte molecules on the electrode surface. On the contrary, if the amount of monomer was excessive, the non-specific interactions occured on the electrode surface instead of the specific interaction of the monomer with the analyte. Hence, CYM imprinted electrodes were produced by 100.0 mmol L^{-1} Py monomer and 25.0 mmol L^{-1} CYM, demonstrating the highest electrochemical signal (Fig. S3B).

Desorption time effect

In prepared MIP-type sensor applications, the analyte molecules deposited on any sensor surface must be removed almost completely from the surface using a desorption solution. If the removal of analyte molecules is insufficient, significant sensitivity problems can occur in the prepared sensors. In this study, the desorption times in the range of 10–50 min were studied, and as seen in Fig. S3C, at the 20 min and later, the analyte molecules were sufficiently removed from the electrode surface and the current signals remained constant and the desorption time of 20 min was chosen as optimum desorption time.

Scan cycle effect

In electrochemical imprinting sensor preparations, the number of CV scans is another important factor affecting sensor sensitivity. A high number of scans results in a thick polymeric layer forming on the electrode surface, making it difficult to remove analyte molecules from the surface. On the contrary, since a thin polymeric layer can be formed, the electrode stability can not be at the desired level. Hence, the optimum scan cycle number of 25 was selected for the development of CYM imprinted polymer on Bi-$BiVO_4$/GCE (Fig. S3D).

Sensitivity of MIP/Bi-$BiVO_4$/GCE and recovery studies

Square wave voltammograms (SWVs) obtained against the CYM analyte at increasing concentrations under optimum experimental conditions using MIP/Bi-$BiVO_4$/GCE electrode were given in Fig. 7. The linearity between CYM concentrations vs. peak signals was obtained in calibration with ($I\ (\mu A) = 0.9253 C_{CYM}$ (nmol L^{-1}) + 0.1811 and regression coefficient value 0.9978 (inset of Fig. 6). LOQ of 1.0×10^{-9} mol L^{-1} and LOD of 3.3×10^{-10} mol L^{-1} (see Supplementary Data for the equations) suggested that the prepared MIP/Bi-$BiVO_4$/GCE electrode for the detection of CYM analyte had a satisfactory sensitivity. To better understand the sensitivity of the prepared sensor comparatively, a comparison was made with the methods developed for other CYM analyses in the literature (Table 1). As can be seen from these results, the prepared sensor showed high sensitivity for CYM analysis. In addition, the waste generation was minimal during the formation of the Bi-$BiVO_4$ nanocomposite using the one-step hydrothermal technique in Sect. 2.3 in comparison with the other methods. This proved that a developed sensor system with an environmentally friendly technique had been successfully presented to the literature. Moreover, because SERS and UPLC techniques for CYM detection were expensive and complex techniques that required high expertise, CYM detection was impractical by using these complex methods. In conclusion, the advantages of the prepared electrochemical sensor, such as its fast response time, will enable early diagnosis of metabolic disorders caused by the exposure to fungicide-type pesticides and faster and more effective analyses of other fungicide-type pesticides will be possible in the coming years through the sensors produced in this study.

Recovery experiments were performed on orange and apple juice samples to demonstrate the applicability of the developed MIP/Bi-$BiVO_4$/GCE sensor with high selectivity

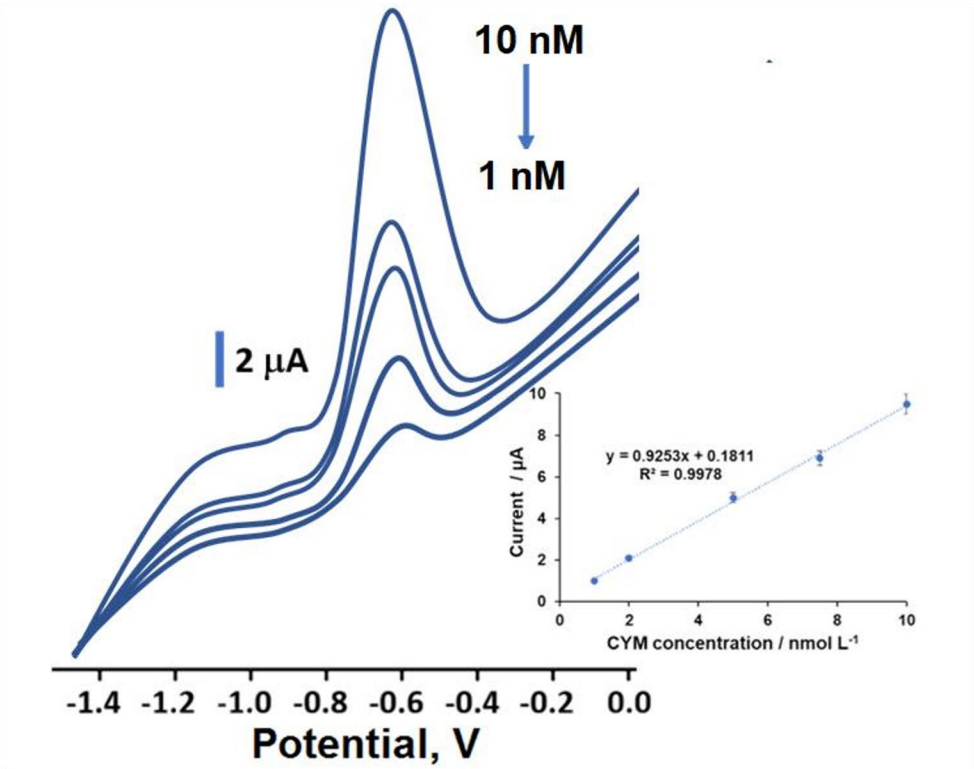

Fig. 6 CYM concentration effect on MIP/Bi-$BiVO_4$/GCE in existence of pH 6.0 of PB (from 1.0×10^{-9} to 1.0×10^{-8} mol L^{-1} CYM) by SWV method. Inset: Calibration curve of CYM concentrations against the current signals

and accuracy in a real sample environment. According to the analytical results shown in Table 2, it was shown that the prepared CYM imprinted electrochemical sensor could determine CYM with high recovery close to 100.00%. As another method, CYM analysis was performed in orange and apple juice samples using the developed analytical method such as HPLC for CYM analysis available in the literature [29]. There were no important differences between MIP/Bi-$BiVO_4$/GCE and HPLC, suggesting another proof of the accuracy of the prepared molecularly imprinting electrochemical sensor.

To confirm the high selectivity and accuracy of the results using the direct calibration technique, the standard addition method [$I\,(\mu A)=0.9288C_{CYM}\,(\text{nmol L}^{-1})+1.0934$] was also applied to orange and apple juice samples, and the slopes of the obtained calibration equations from these two techniques were compared. Consequently, there were no crucial differences between the slopes, verifying the reliability of the prepared MIP sensor in this study. In addition, the other potential interferents (ascorbic acid, sugars, phenolics) did not negatively affect the analysis results and sensor selectivity.

Table 1 The comparison of MIP/Bi-$BiVO_4$/GCE's analytical performance with the studied methods in literature

Method	Linear range (mol L^{-1})	LOD (mol L^{-1})	Real sample	Ref.
TAT-AgNPs	1.0×10^{-6} – 1.0×10^{-4}	1.3×10^{-8}	Tap water and river water	[30]
SERS	5.3×10^{-6} – 2.6×10^{-4}	2.6×10^{-6}	-	[31]
NB-Gr/GC electrode LSV	4.0×10^{-5} – 1.0×10^{-3}	1.2×10^{-5}	Various vegetables and fruits	[13]
Dual-channel ratiometric colorimetry + FL (CDs/AgNPs)	1.0×10^{-8} – 5.5×10^{-7}	2.0×10^{-9}	Natural river water, soil and plant epidermis	[32]
Square-Wave Stripping Voltammetry (SWSV) + Cyclic Voltammetry (CV)	1.2×10^{-7} – 8.5×10^{-6}	3.6×10^{-8}	River water	[33]
Ultra-Performance Liquid Chromatography – Photodiode Array Detection (UPLC–PDA)	5.0×10^{-7} – 2.5×10^{-5}	1.5×10^{-8}	Pepper	[7]
MIP/Bi-$BiVO_4$/GCE	1.0×10^{-9} – 1.0×10^{-8}	3.3×10^{-10}	Orange and apple juice	This study

Selectivity, stability and reproducibility of MIP/Bi-$BiVO_4$/GCE

To reveal the high selectivity of MIP/Bi-$BiVO_4$/GCE, the developed molecularly imprinting sensor was treated with CYM and the other interfering agents such as CYP, MAN, MET and SPI (Fig. 7). According to Fig. 7, CYM-specifically

Table 2 Recovery results of CYM ($n=6$)

MIP/Bi-$BiVO_4$/GCE				HPLC	
Sample	Added CYM (nmol L^{-1})	Found CYM (nmol L^{-1})	*Recovery (%)	Found CYM (nmol L^{-1})	*Recovery (%)
Orange juice	-	3.12 ± 0.04	-	3.13 ± 0.03	-
	2.00	5.12 ± 0.01	100.00 ± 0.02	5.13 ± 0.03	100.00 ± 0.03
	4.00	7.13 ± 0.01	100.14 ± 0.04	7.14 ± 0.01	100.14 ± 0.03
	6.00	9.11 ± 0.05	99.89 ± 0.01	9.14 ± 0.06	100.11 ± 0.04
Apple juice	-	2.07 ± 0.02	-	2.06 ± 0.02	-
	2.00	4.07 ± 0.03	100.00 ± 0.01	4.08 ± 0.04	100.49 ± 0.02
	4.00	6.08 ± 0.03	100.17 ± 0.01	6.09 ± 0.04	100.50 ± 0.01
	6.00	8.06 ± 0.04	99.88 ± 0.03	8.07 ± 0.05	100.12 ± 0.03

*Recovery = Found CYM, nmol L^{-1} / Real CYM, nmol L^{-1}

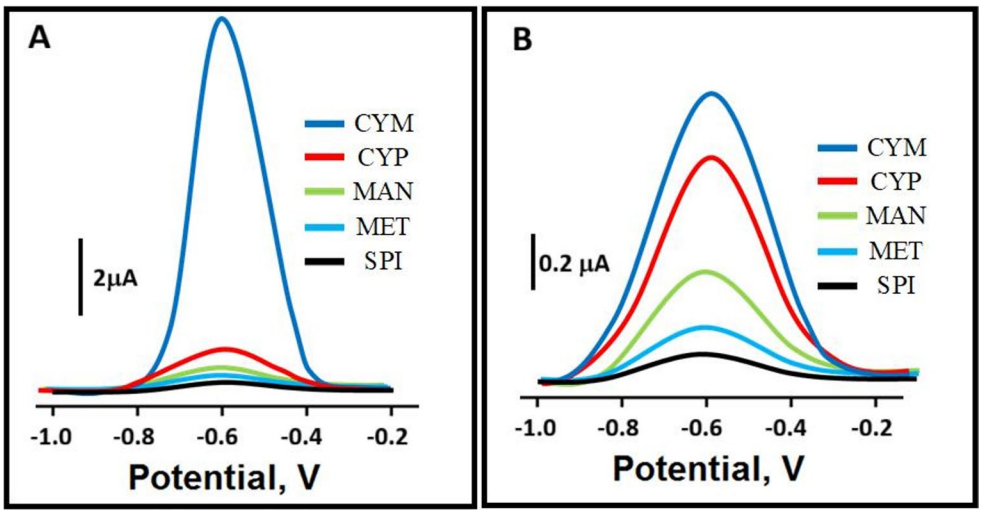

Fig. 7 SWVs of (**A**) MIP/Bi-$BiVO_4$/GCE and (**B**) NIP/Bi-$BiVO_4$/GCE in 10.0 nmol L^{-1} CYM, 1000.0 nmol L^{-1} CYP, 1000.0 nmol L^{-1} MAN, 1000.0 nmol L^{-1} MET and 1000.0 nmol L^{-1} SPI in 0.1 M PB (pH 6.0)

prepared sensor was shown to exhibit the highest electrochemical activity to CYM as expected. MIP/Bi-$BiVO_4$/GCE was proven to recognize CYM 9.50 times more selectively than CYP, 19.00 times more selectively than MAN, 31.67 times more selectively than MET and 47.50 times more selectively than SPI (Table S1). Consequently, the high values of the selectivity coefficient (k) and relative selectivity coefficient (k') confirmed the preparation of highly selective molecularly imprinting sensor for CYM and its successful application.

For the stability of MIP/Bi-$BiVO_4$/GCE sensor, the prepared sensor was interacted with 10.0 nmol L^{-1} CYM for 9 weeks and the electrochemical signal values were recorded (Fig. S4). The measurements of the peak current signals over 9 weeks were close to each other, indicating the high stability of the prepared sensor. For the reproducibility test of MIP/Bi-$BiVO_4$/GCE, 15 different MIP/Bi-$BiVO_4$/GCE electrodes were prepared in harmony with Sect. 2.4 and 2.5. In existence of 10.0 nmol L^{-1} CYM, the relative standard deviation value of obtained 15 electrochemical signals was 0.66%, revealing the high reproducibility of MIP/Bi-$BiVO_4$/GCE.

Conclusions

Herein, a novel molecularly imprinted electrochemical determination of cymoxanil fungicide by using bismuth incorporated bismuth vanadate nanocomposite was presented for the first time in the literature. The bismuth incorporated bismuth vanadate nanocomposite showed the increased electrochemical signals, resulting from the synergistic combination of bismuth and bismuth vanadate. Furthermore, the developed MIP based sensor demonstrated the high selectivity towards cymoxanil fungicide in presence of the other chemical agents and LOQ of 1.0×10^{-9} mol L^{-1} and LOD of 3.3×10^{-10} mol L^{-1} confirmed the high sensitivity of the prepared electrochemical sensor. Finally, this sensor was applied to cymoxanil fungicide detection in orange and apple juice samples with high recovery.

Supplementary Information The online version contains supplementary material available at https://doi.org/10.1007/s00604-025-07745-2.

Author contributions Şule Yıldırım Akıcı: Conceptualization, Methodology, Writing - review & editing. Sena Bekerecioğlu: Data curation, Visualization, Investigation. İlknur Polat: Data curation, Visualization, Investigation. Müge Mavioğlu Kaya: Conceptualization,

Methodology, Writing - review & editing. Necip Atar: Data curation, Visualization, Investigation. Mehmet Lütfi Yola: Supervision, Conceptualization, Writing - review & editing.

Funding This research received no external funding.

Data availability No datasets were generated or analysed during the current study.

Declarations

Ethical approval This research did not involve human or animal samples.

Competing interests The authors declare no competing interests.

References

1. Song X, Corlett RT, Yang J, Luskin MS (2025) Fungicide effects on wild plants: insights from a global meta-analysis. New Phytol 248(3):1491–1500
2. Rekanović E, Potočnik I, Milijašević-Marčić S, Stepanović M, Todorović B, Mihajlović M (2012) Toxicity of metalaxyl, azoxystrobin, dimethomorph, cymoxanil, Zoxamide and mancozeb to phytophthora infestans isolates from Serbia. J Environ Sci Health Part B 47(5):403–409
3. Balkan T, Kara K (2023) Dissipation kinetics of some pesticides applied singly or in mixtures in/on grape leaf. Pest Manag Sci 79(3):1234–1242
4. González Álvarez M, Noguerol-Pato R, González-Barreiro C, Cancho-Grande B, Simal-Gándara J (2012) Changes of the sensorial attributes of white wines with the application of new anti-mildew fungicides under critical agricultural practices. Food Chem 130(1):139–146
5. Herrero-Hernández E, Andrades MS, Marín-Benito JM, Sánchez-Martín MJ, Rodríguez-Cruz MS (2011) Field-scale dissipation of Tebuconazole in a vineyard soil amended with spent mushroom substrate and its potential environmental impact. Ecotoxicol Environ Saf 74(6):1480–1488
6. Authority EFS (2015) Review of the existing maximum residue levels for Cymoxanil according to Article 12 of regulation (EC) 396/2005. EFSA J 13(12):4355
7. Liu X, Yang Y, Cui Y, Zhu H, Li X, Li Z, Zhang K, Hu D (2014) Dissipation and residue of Metalaxyl and Cymoxanil in pepper and soil. Environ Monit Assess 186(8):5307–5313
8. Ahmed MS, Massoud AH, Derbalah AS, Al-Brakati A, Al-Abdawani MA, Eltahir HA, Yanai T, Elmahallawy EK (2020) Biochemical and histopathological alterations in different tissues of rats due to repeated oral dose toxicity of Cymoxanil. Animals 10(12):2205
9. Huang Y, Chen Z, Meng Y, Wei Y, Xu Z, Ma J, Zhong K, Cao Z, Liao X, Lu H (2020) Famoxadone-cymoxanil induced cardiotoxicity in zebrafish embryos. Ecotoxicol Environ Saf 205:111339
10. Morrica P, Fidente P, Seccia S (2005) High-performance liquid chromatographic mass spectrometric identification of the photoproducts of Cymoxanil. Biomed Chromatogr 19(7):506–512
11. Kanario M, Matofari JW, Nduko JM (2025) Influence of On-farm pesticide practices and processing methods on pesticide residue levels in potato tubers (Solanum tuberosum L.) in Nyandarua County, Kenya. J Food Prot 88(7):100521
12. Cabizza M, Dedola F, Satta M (2012) Residues behavior of some fungicides applied on two greenhouse tomato varieties different in shape and weight. J Environ Sci Health Part B 47(5):379–384
13. Varodi C, Pogăcean F, Coros M, Magerusan L, Stefan-van Staden R-I, Pruneanu S (2021) Hydrothermal synthesis of Nitrogen, Boron Co-Doped graphene with enhanced Electro-Catalytic activity for Cymoxanil detection. Sensors 21(19):6630
14. Zhou Y, Tian M, Li R, Zhang Y, Zhang G, Zhang C, Shuang S (2023) Ultrasensitive electrochemical platform for dopamine detection based on CoNi-MOF@ERGO composite. ACS Biomaterials Sci Eng 9(10):5599–5609
15. Mourzina YG, Ermolenko YE, Offenhäusser A (2021) Synthesizing electrodes into electrochemical sensor systems. Front Chem 9:13
16. Song K, Liu H, Chen B, Gong C, Ding J, Wang T, Liu E, Ma L, Zhao N, He F (2024) Toward efficient utilization of photogenerated charge carriers in photoelectrochemical systems: engineering strategies from the atomic level to configuration. Chem Rev 124(24):13660–13680
17. Feng L, Li X, Wang J, Chen E, Fan Y, Jin L, Tang P, Zhang L (2025) Metallic Bi-decorated BiVO4 nanosheets enabling improved photoelectrochemical detection of trace Chlorpyrifos under visible light through localized surface plasmon resonance. Microchim Acta 192(11):728
18. Thirumalraj B, Jaihindh DP, Alaswad SO, Sudhakaran MSP, Selvaganapathy M, Alfantazi A, Choe H, Kwon K (2022) Fabricating BiOCl/BiVO4 nanosheets wrapped in a graphene oxide heterojunction composite for detection of an antihistamine in biological samples. Environ Res 212:113636
19. Cheng X, Li D, Jiang Y, Huang F, Li S (2024) Advances in electrochemical energy storage over metallic Bismuth-Based materials. Materials 17(1):21
20. El-Schich Z, Zhang Y, Feith M, Beyer S, Sternbæk L, Ohlsson L, Stollenwerk M, Wingren AG (2020) Molecularly imprinted polymers in biological applications. Biotechniques 69(6):407–420
21. Piletsky S, Canfarotta F, Poma A, Bossi AM, Piletsky S (2020) Molecularly imprinted polymers for cell recognition. Trends Biotechnol 38(4):368–387
22. Yola ML, Atar N, Qureshi MS, Üstündağ Z, Solak AO (2012) Electrochemically grafted Etodolac film on glassy carbon for Pb(II) determination. Sens Actuators B 171:1207–1215
23. Liu J, Yang X, Si F, Zhao B, Xi X, Wang L, Zhang J, Fu X-Z, Luo J-L (2022) Interfacial component coupling effects towards precise heterostructure design for efficient electrocatalytic water splitting. Nano Energy 103:107753
24. Yuan R, Liu Q, Hong H, Ma H, Xiao L, Li Y, Jiang D, Hao N, Wang K (2022) Enhanced cathodic electrochemiluminescent microcystin-LR aptasensor based on surface plasmon resonance of Bi nanoparticles. J Hazard Mater 434:128877
25. Wang M, Guo P, Zhang Y, Liu T, Li S, Xie Y, Wang Y, Zhu T (2018) Eu doped g-C3N4 nanosheet coated on flower-like BiVO4 powders with enhanced visible light photocatalytic for Tetracycline degradation. Appl Surf Sci 453:11–22
26. Sun M, Zhang W, Sun Y, Zhang Y, Dong F (2019) Synergistic integration of metallic Bi and defects on bioi: enhanced photocatalytic NO removal and conversion pathway. Chin J Catal 40(6):826–836
27. Shuai Y, Peng R, He Y, Liu X, Wang X, Guo W (2023) NiO/BiVO4 p-n heterojunction microspheres for conductometric triethylamine gas sensors. Sens Actuators B 384:133625
28. Brito JFd, Corradini PG, Zanoni MVB, Marken F, Mascaro LH (2021) The influence of metallic Bi in BiVO4 semiconductor for artificial photosynthesis. J Alloys Compd 851:156912
29. López de Sabando O, Gómez de Balugera Z, Goicolea MA, Rodríguez E, Sampedro MC, Barrio RJ (2002) Determination of Simazine and Cymoxanil in soils by microwave-assisted solvent extraction and HPLC with reductive amperometrical detection. Chromatographia 55(11):667–671

30. Ali I, Khan S, Ali Shah Z, Ahmed F, Shah I, Hameed A, Ullah R, Raza Shah M (2024) Synthesis and characterization of silver nanoparticles conjugated with Triazole-N-acetamide thiazole derivatives for selective detection of Cymoxanil in complex samples. ChemistrySelect 9(4):e202304484
31. Mi S, Ji L, Yu H, Guo Y, Cheng Y, Yang F, Yao W, Xie Y (2021) Zero-Background Surface-Enhanced Raman scattering detection of Cymoxanil based on the change of the cyano group after ultraviolet irradiation. J Agric Food Chem 69(1):520–527
32. Jiang X, Jin H, Sun Y, Gui R (2019) Colorimetric and fluorometric dual-channel ratiometric determination of fungicide Cymoxanil based on analyte-induced aggregation of silver nanoparticles and dually emitting carbon Dots. Microchim Acta 186(8):580
33. Mercan H, İnam R (2010) Determination of Cymoxanil fungicide in commercial formulation and natural water by Square-wave stripping voltammetry. CLEAN – Soil Air Water 38(5–6):558–564